Physics – Uspekhi **59** (2) 174 – 183 (2016)

CONFERENCES AND SYMPOSIA

PACS numbers: 03.75.Lm, 05.30.Fk, **67.85.–d**, **74.78.–w**

Fermi liquid-to-Bose condensate crossover in a two-dimensional ultracold gas experiment

T V Barmashova, K A Martiyanov, V B Makhalov, A V Turlapov

DOI: 10.3367/UFNe.0186.201602i.0183

Contents

Abstract. By controling interparticle interactions, it is possible to transform a fermionic system into a bosonic system and vice versa, while preserving quantum degeneracy. Evidence of such a transformation may be found by monitoring the pressure and interference. The Fermi pressure is an indication of the fermionic character of a system, while the interference implies a nonzero order parameter and Bose condensation. Lowering from three to two spatial dimensions introduces new physics and makes the system more difficult to describe due to the increased fluctuations and the reduced applicability of mean field methods. An experiment with a two-dimensional ultracold atomic gas shows a crossover between the Bose and Fermi limits, as evident from the value of pressure and from the interference pattern, and provides data to test models of 2D Fermi and Bose systems, including the most-difficult-to-model strongly coupled systems.

Keywords: ultracold atomic and molecular gases, Bose gas, Fermi gas, Fermi-to-Bose crossover, Fermi liquid, Bose–Einstein condensation, matter-wave interference

T V Barmashova, K A Martiyanov, V B Makhalov
Institute of Applied Physics, Russian Academy of Sciences,
ul. Ul'yanova 46, 603000 Nizhny Novgorod, Russian Federation
A V Turlapov Institute of Applied Physics, Russian Academy of Sciences,
ul. Ul'yanova 46, 603000 Nizhny Novgorod, Russian Federation;
N I Lobachevsky State University of Nizhni Novgorod,
prosp. Gagarina 23, 603950 Nizhny Novgorod, Russian Federation
E-mail: turlapov@appl.sci-nnov.ru

Received 1 December 2015
Uspekhi Fizicheskikh Nauk **186** (2) 183 – 192 (2016)
DOI: 10.3367/UFNr.0186.201602i.0183
Translated by A V Turlapov; edited by A Radzig

1. Introduction

Ideas about the quantum degeneracy of fermions [1, 2] and the condensation of bosons [3] were formulated at nearly the same time. The paths to understanding the physical significance of these concepts turned out to be quite different. Ideas about the low-temperature behavior of fermions were immediately employed in explaining the heat capacity of metals [4]. A system suitable for testing the ideas of Bose condensation appeared only 10 years later. Following the P L Kapitza report about the helium superfluidity [5], Fritz London conjectured that the superfluidity is connected to Bose condensation [6, 7]. Today, this point of view seems natural. According to the theory of those days, however, the Bose condensate could not be superfluid. Only the ideal Bose gas condensate was known then. Its dispersion relation is quadratic and, therefore, does not satisfy the Landau superfluidity criterion [8], which requires either linear or convex dependence of the energy on the momentum.

The situation changed only in 1947, when Bogoliubov showed that any weak coupling makes the dispersion relation linear at low momenta, meaning that the Bose gas becomes superfluid [9]. Later on, it was established that a noninteracting Bose gas does not even undergo a phase transition in Landau's sense, because no order parameter appears [10]. Therefore, interactions are what makes Bose-gas physics interesting.

Moreover, by tuning the interactions in a system, one may drastically change the quantum statistics from bosonic to fermionic and vice versa. On the one hand, such a problem may look trivial: indeed, nearly all know bosons are composed of fermions, just as the hydrogen atom consists of a proton and electron, and, seemingly, ionization resolves the problem of creating two Fermi systems from a hydrogen

condensate. However, such systems would hardly be degenerate and, moreover, stable. For example, electrons will not have enough room in the momentum space upon monochromatic excitation of a uniform condensate.

To convert a degenerate bosonic system into a fermionic one and vice versa, smooth control of interactions is necessary. This issue was first considered by Keldysh and Kozlov [11] in 1968 for a gas of excitons which substantially overlap upon small electron–hole coupling and transform into a gas of point-like bosons as the coupling increases.

In the 1980s, it became clear that the smooth transform of a Fermi gas into a Bose condensate is already contained in the Bogoliubov superconductivity theory [12, 13]. Even with infinitely small attraction, fermions with opposite spins form Cooper pairs. In response to adiabatically increasing attraction, the pairs contract and smoothly cross over into point-like bosons, as described, for example, in Ref. [14]. Such a transformation of a fermionic system into a bosonic one is a principally many-body effect. Initially, the bond in the pairs appears due to the presence of the Fermi surface. Only after the interaction strength overcomes a threshold does the bound state become stable in the vacuum. The bound-state emergence is not accompanied by any jumps in system properties. Such a change in the statistics has been considered not only for excitons but also for electrons in superconductors and for quark matter [15]. Physical implementation of the phenomenon was realized in an experiment with an ultracold gas of Fermi atoms [16].

In a two-dimensional system, a bound state always exists in the case of attractive interaction of two particles even in the vacuum: infinitely small interaction may bind two fermions into a boson. Nevertheless, the problem of crossover between Bose and Fermi statistics naturally appears in a many-body two-dimensional system. Such a crossover is schematically shown in Fig. 1. In cases where the vacuum bound-state size is larger than the interparticle distance, the system looks like a gas of fermions. Upon contraction of the bound-state to a size much smaller than the interparticle distance, the system becomes bosonic. Between the fermionic and bosonic limits lies the region of strong many-body interactions, where the size of fermion pairs is comparable to the interparticle distance.

In two-dimensional uniform systems, long-range order does not appear at finite temperatures due to thermal fluctuations of the order parameter. In particular, this prohibits Bose condensation. Nevertheless, the reduction of the spatial dimensionality from three to two does not impoverish many-body physics, but makes it more diverse. New phase transitions appear [17–21]. For example, the superfluid phase is destroyed at the Berezinskii–Kosterlitz–Thouless (BKT) transition [17, 18] via the appearance of pairs of vortices with opposite circulations. The role of interactions in the BKT transition is even clearer than in the Bose condensation in the three-dimensional space: for vanishing coupling, the critical temperature goes to zero, though logarithmically [22].

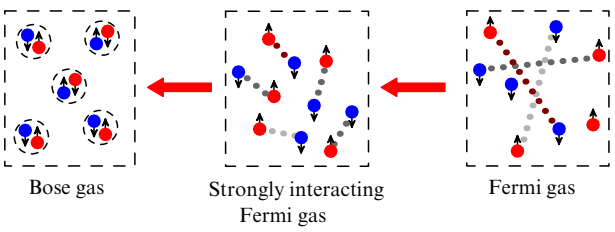

Figure 1. (Color online.) Sizes of fermion pairs at different stages of the crossover between the Fermi (on the right) and Bose (on the left) statistics.

The BKT transition became the first-known phase transition with nontrivial topology. Presently, topological phase transitions in two-dimensional systems are actively being studied [19–21]. Other examples of interesting physics in two dimensions include the integer [23] and fractional [24] quantum Hall effects.The high-temperature superconductivity observed in materials with two-dimensional kinematics has yet to be explained [25].

In two-dimensionality, a description of the Fermi-to-Bose crossover turned out to be nontrivial. Such a unified theory has to describe weakly interacting Fermi and Bose gases, as well as the systems in the intermediate strongly interacting regime. Two-dimensional systems differ from three-dimensional ones: in the former, the mean-field model applicability is limited because according to the Ginzburg–Levanyuk criterion [26, 27], the precision of mean-field approximations decreases with decreasing dimensionality. For example, the mean-field model of Cooper pairs, unlike in three dimensions, yields a qualitatively incorrect solution for thermodynamic properties, e.g., predicting that the Fermi pressure is present in the bosonic limit. Descriptions of the crossover free from such qualitative contradictions appeared just recently [28–33]. The results of such calculations, however, contain significant quantitative discrepancies.

Construction of a quantitatively correct two-dimensional theory is of practical significance at least in two cases:

— first, to explain high-temperature superconductivity in layered systems where the Cooper pair size is comparable to the interparticle distance, as in the strongly interacting regime of the Bose-to-Fermi crossover problem. Noted models account for s-wave coupling only, while the d-wave symmetry dominates in the superconducting phase of the cuprates. Despite that, models with s-wave coupling are also important because the s-wave symmetry has been detected in the pseudogap phase of cuprate superconductors [34];

— second, to understand the dynamics of neutron stars where the so-called nuclear lasagna phase may exist. The nuclear lasagna is an area consisting of strongly interacting fermions with predominantly two-dimensional kinematics, possibly limiting the rotation period of pulsars [35].

Therefore, the problem of two-dimensional Fermi system behavior, especially in the strongly interacting regime, is important. Furthermore, there is an interesting question of condensation of bosonic particles in finite-size systems with strong repulsion between bosons.

Description of interactions is a common question for kinematically two-dimensional systems. In the high-temperature superconductivity theory, for example, purely two-dimensional models are frequently used [36]. These models assume motion along the xy plane and independence of interactions from z. An example where such a pure two-dimensional model is insufficient is ^{3}He on a substrate: the increase in zero-point oscillations relative to the interaction radius brings about formation of a self-bound liquid [37]. A unified and correct description of interactions in all regimes is required during construction of a model for a system with tunable statistics. Experiments with such a system may test the applicability of purely two-dimensional models to real systems.

A two-dimensional ultracold gas of Fermi atoms [38], similarly to the three-dimensional one, allows broad tunability of s-wave interactions. Because of this, the properties of two-dimensional Fermi gases have been studied in different modes. It has been found that a reduction in the kinematic dimensionality indeed favors pairing of the particles [39, 40]. Thermodynamic properties have been measured at nearly zero [41, 42] and finite [42, 43] temperatures.

This paper is devoted to the crossover of a two-dimensional system between the Fermi and Bose limits. For the role of the experimental system, an ultracold gas of fermionic lithium-6 atoms is chosen. Evidence of such a crossover may be found by monitoring the pressure in the gas and by observing the interference. Fermi pressure tells us about the fermionic character of the system, while the interference indicates the appearance of the order parameter and condensation of diatomic bosonic molecules.

The paper outline is as follows. In Section 2, we discuss the properties of ultracold quantum gas that make these gases an attractive research subject; we also describe the spin states of Fermi atoms and a means for establishing two-dimensional kinematics. Section 3 is devoted to the control of interactions and their parameterization. In Section 4, we explain how the crossover between Fermi and Bose statistics is observed in the pressure. Section 5 is devoted to condensation of Bose molecules. In Section 6, we discuss available models of the crossover and compare predictions of such models with measured pressure.

2. Two-dimensional gas of lithium atoms in optical dipole traps

2.1 Ultracold quantum gases

Experiments with ultracold quantum gases have allowed observing states of matter and effects that were previously just a matter of theoretical discussions: Bogoliubov weakly interacting Bose gas [44], Bertsch fermionic matter with resonantly strong attraction [45], crossover between the fermionic Bardeen–Cooper–Schrieffer superfluidity and Bose condensation [16], Tonks–Girardeau fermionization of a one-dimensional Bose gas [46], and Efimov trimers [47]. Ultracold gases are involved for quantitative tests of theories that are applicable to condensed matter, high-energy and nuclear physics [48, 49].

The success of experiments is facilitated by a set of unique conditions:

— uncontrolled impurities are absent in ultracold gases, because the gas preparation is done by spectroscopic methods that are sensitive not only to chemical elements but also to isotope composition;

— both the interactions and the spin composition may be tuned smoothly and reversibly;

— kinematic dimensionality is controlled;

— measurements are performed directly: it is possible to instantaneously image the density distribution owing to absorption of light by the atomic gas, to measure thermodynamic properties, and to observe the momentum spatial distribution and the difference between the order parameter phases of subsystems.

Achievement of quantum degeneracy requires cooling to temperature T of micro- to nanokelvin range. In the simplest case, the atomic gas is prepared in two stages, taking a few seconds each. At the first stage, the trapping and cooling of

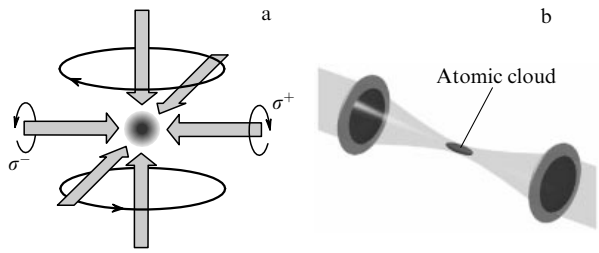

Figure 2. (a) Trapping and cooling of an atomic gas in a magneto-optical trap. Six trapping beams, two magnetic coils with opposite currents, and the atomic cloud are shown. (b) Confinement of an atomic cloud in an optical dipole trap formed by the focus of a laser beam.

atoms is performed using laser radiation with a frequency close to the resonance [50]. The gas is collected in a magneto-optical trap from either an atomic beam or ambient vapor. The trap is schematically depicted in Fig. 2a. By means of the viscous light pressure force, whose value is adjusted by the Zeeman shift, the atomic gas is gathered near the point where the magnetic field is zero.

The trap collects from millions to billions of atoms. Their state is far from quantum degeneracy. For example, the phase space density is just $\sim 10^{-6}$ for the lithium used in this work. Further cooling is impossible due to the resonant light used at this stage. Due to reemission of photons, there appears a temperature minimum which is a few tens of microkelvins for lithium. Moreover, a further increase in the density is prevented by the light pressure of the atoms upon each other, appearing due to the reemission. Therefore, the next stage of cooling is needed. At the start of this stage, the resonant light fields are instantaneously extinguished, and the atomic gas finds itself in a conservative potential which is produced by a nonresonant electric or magnetic field.

The optical dipole trap [51] in the simplest case is created in the focus of a laser beam, as shown in Fig. 2b. The radiation frequency is tuned far below the electrodipole transitions in the atom which is held back by potential $V = -(1/2)\mathbf{dE}$, where $\mathbf{E}$ is the electric field, and $\mathbf{d} \propto \mathbf{E}$ is the induced dipole moment. The potential is conservative due to the large detuning between the laser frequency and the atomic transition frequency. In the optical dipole trap, the magnetic field remains a free parameter and may be used to control the interaction among the particles (see Section 3.1).

Further cooling is done by means of evaporation [52]. Particles with the highest energies leave the trap, while the remaining particles collide and attempt to form an equilibrium distribution at a lower temperature. This repopulates the higher momentum states, which again brings about losses of the energetic particles. To speed up the evaporation, the trap depth is slowly decreased. As a result, the cooling brings the gas into a degenerate state with the phase space density of ~ 1.

The ultracold quantum gases are extremely dilute. The interparticle distance ranges between hundreds of nanometers and several microns, which is much larger than the intermolecular distance of 3 nm in the air and the typical scale of the interatomic potentials: $r_0 \sim 0.1-1$ nm. At the same time, it is possible to speak about the collective behavior typical of fluids: parts of the system feel each other at large distances due to the appearance of a collective wave function or due to the Pauli exclusion principle; similarly to fluids, strong interparticle interactions, whose energy is comparable

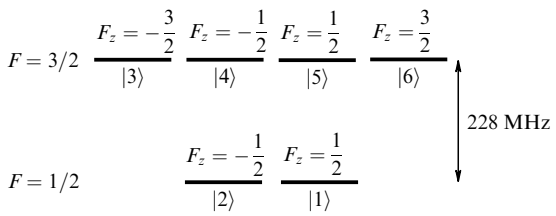

Figure 3. Spin states of lithium-6 in a zero magnetic field, $B = 0$, which correspond to the ground state of the valence electron $2^2S_{1/2}$. The states are numbered in the order of increasing energy in the magnetic field.

to the kinetic energy, may appear [53]. Finally, the Fermi gas with weak attraction provides an example of a Fermi liquid in the Landau sense. Moreover, this is one of a few systems where the Fermi-liquid parameters are computed from first principles [54].

2.2 Spin states of Fermi atoms

The spin degree of freedom is fundamental to the properties of Fermi systems. The role of spin in atomic gas is played by the internal state of the atom. In experiments described below, the lithium-6 atom is used. Together with potassium-40, this is one of the two most popular atoms in Fermi gas experiments. The states of lithium-6 corresponding to the ground-state orbital of the single valence electron $2s^1$ are shown in Fig. 3. These states differ by the mutual orientation of the valence-electron spin $S = 1/2$ and the nuclear spin $I = 1$. In the absence of the magnetic field, the states may be expanded in the basis of the total angular momentum operator $\hat{\mathbf{F}} = \hat{\mathbf{S}} + \hat{\mathbf{I}}$. The mixture of states $|1\rangle$ and $|2\rangle$ is an analog of the gas of spin-up and spin-down electrons in a solid body. Problems requiring more spin diversity may be implemented using a gas of lithium-6, as one may see from Fig. 3.

In the experiment, an equal mixture of states $|1\rangle$ and $|2\rangle$ is used. In the external magnetic field B, which is turned on for controling the interactions, the states are expanded in the basis $|S_z, I_z\rangle$ [55]:

$$|1\rangle = \cos\theta_+ \left|-\frac{1}{2}, 1\right\rangle - \sin\theta_+ \left|\frac{1}{2}, 0\right\rangle, \tag{1}$$

$$|2\rangle = \cos\theta_- \left|-\frac{1}{2}, 0\right\rangle - \sin\theta_- \left|\frac{1}{2}, -1\right\rangle, \tag{2}$$

where

$$\sin\theta_\pm = \frac{1}{\sqrt{1 + (Z^\pm + R^\pm)^2/2}},$$

$$Z^\pm = \frac{2\mu_B B}{\alpha} \pm \frac{1}{2}, \qquad R^\pm = \sqrt{(Z^\pm)^2 + 2},$$

μ_B is the Bohr magneton, and $\alpha/(2\pi\hbar) = 152.1$ MHz is the hyperfine interaction constant. In the field of $B = 600$–1000 G, typical for the experiment, first terms of states (1) and (2) dominate. These terms correspond to projection $S_z = -1/2$. At $B = 800$ G, for example, $\sin^2\theta_\pm = 0.002$. Despite this, the part of the state corresponding to projection $S_z = 1/2$ is fundamental to the tunability of the interactions.

2.3 Two-dimensional kinematics

In the experiment, the gas clouds are held in a series of traps, as shown in Fig. 4a schematically. The trapping potential is produced by a standing wave of radiation with wavelength $\lambda = 10.6$ μm, which gives a 5.3 μm of distance between the antinodes and, as a result, lets us resolve each cloud in the images.

An image of the clouds made along the xy plane of motion is shown in Fig. 4b, where each light strip is a separate two-dimensional system. To take this snapshot, the clouds are shined upon by monochromatic radiation of wavelength 671 nm, which is resonant to the electric dipole transition $2S_{1/2} \to 2P_{3/2}$ in the lithium-6 atom. As a result of the resonant absorption, a shadow appears and is further projected onto a charge coupled device. The absorption lets us reconstruct the gas density distribution integrated along y-axis [38, 41]. Such photography is selective to the internal atomic state. The imaging destroys the state of the system due to the energy input, which is much larger than the Fermi energy. Preparing a few dozen clouds in identical conditions allows, first, averaging the data over the ensemble for the sake of noise suppression and, second, observing interference.

Near the bottom of each trap, the confining potential is close to a harmonic one:

$$V(x, y, z) = \frac{m\omega_z^2 z^2}{2} + \frac{m\omega_x^2 x^2}{2} + \frac{m\omega_y^2 y^2}{2}, \quad \omega_z \gg \omega_x, \omega_y, \tag{3}$$

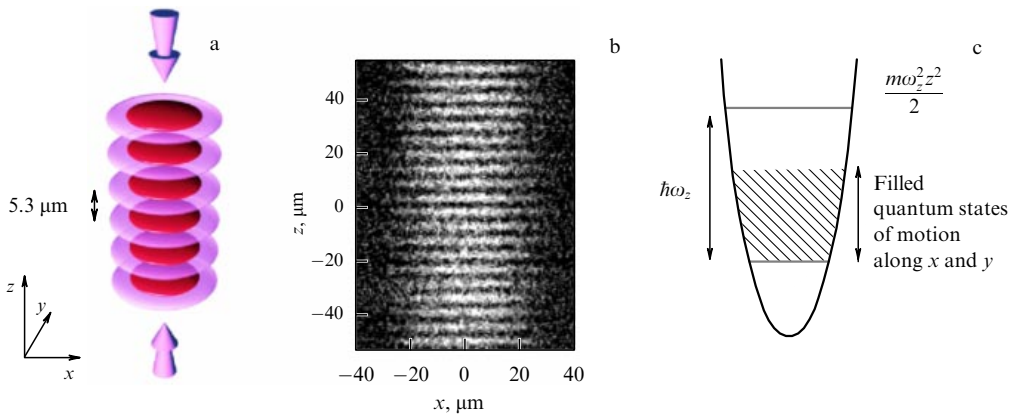

Figure 4. (Color online.) (a) Confinement of two-dimensional gas clouds in antinodes of a standing electromagnetic wave. The gas is shown in dark red, while the intensity of the radiation forming the trap is shown in light purple. (b) Image of the clouds along the y direction. (c) Two-dimensional ideal Fermi gas at $T = 0$, whose motion is quantized along z- and nearly free along x- and y-axes.

where m is the atom mass. Due to the strong trap anisotropy, $\omega_z \gg \omega_\perp \equiv \sqrt{\omega_x \omega_y}$, it is possible to put the absolute majority of the atoms into the ground state of motion along the z-axis, while, according to the Pauli exclusion principle, the fermions populate many states of motion in the xy plane, as shown in Fig. 4c. As a result, the gas is kinematically two-dimensional. In Fig. 4b, the gas clouds reside in a potential with frequencies of $\omega_x/(2\pi) = \omega_y/(2\pi) = 102$ Hz, $\omega_z/(2\pi) = 5570$ Hz. The number of atoms in a single cloud per spin state is $N = 660$, which gives the Fermi energy $E_F = \hbar\omega_\perp\sqrt{2N} = 0.67\hbar\omega_z$ and, together with deep degeneracy, nearly excludes thermal population of the excited states of motion along the z-axis.

3. Tunable interparticle interactions

3.1 Tuning the interactions by means of the Feshbach resonance for three-dimensional kinematics

Initially, we consider control of interactions for atoms that freely move in three dimensions, while in Section 3.2 we show how restriction of spatial dimensionality affects the interactions.

Since the kinetic energy is small, it is sufficient to keep just the s-wave term in the partial wave expansion of the interaction. In this approximation, only the atoms in different internal states collide, e.g., in states $|1\rangle$ and $|2\rangle$ for lithium-6. The scattering length a may be tuned to any value by adjusting the external magnetic field B using the Fano–Feshbach resonances [56].

The appearance of the resonance and tunability of the scattering length are illustrated in Fig. 5. At the interaction of two univalent atoms, the valence electrons are found in a superposition of the triplet state with collinear spins, and a singlet state with opposite spins. Different potentials of interparticle interaction, $V_{\text{triplet}}(r')$ and $V_{\text{singlet}}(r')$, respectively, correspond to the triplet and singlet states of the pair. These potentials are depicted in Fig. 5. The external magnetic field B shifts the zero level of the triplet-state kinetic energy, because the state has a large magnetic moment of about $2\mu_B$. If the energy of the unbound state of the pair, shown by the gray dashed line, becomes equal to the singlet-channel bound-state energy (black dashed line), then a scattering resonance appears: in the case of zero kinetic energy, the scattering length diverges to ∞. By detuning bound and free states from each other, any desired scattering length between $-\infty$ and $+\infty$ may be obtained. Near the resonance, an approximate formula may be devised for the s-wave scattering length of two unbound particles:

$$a(B) = a_{\text{bg}}\left(1 + \frac{\Delta}{B - B_0}\right), \tag{4}$$

where B_0 and Δ are the center location and the width of the resonance, respectively, while a_{bg} is the background scattering length stemming from the triplet channel alone. In experiments, the Feshbach resonance with parameters $B_0 = 832$ G, $\Delta = 262$ G, $a_{\text{bg}} = -1580a_0$ (a_0 is the Bohr radius) [57] was employed. Notice that in such a strong magnetic field, the triplet-state part of the electronic spin dominates in the state of the pair of atoms $|1\rangle$ and $|2\rangle$ [see formulas (1) and (2)], because coefficients $\sin\theta_\pm$ are small. The presence of a singlet part, even if small, in the state of electronic spins is fundamental to the coupling of the channels $V_{\text{singlet}}(r)$ and $V_{\text{triplet}}(r)$, the tunability of the interactions, and the appearance of the resonance.

In a many-body system, the Fermi atoms are joined into diatomic molecular bosons by tuning the interactions. For this purpose, the magnetic field smoothly changes from larger values, where the bound state is above the energy of the free state in the triplet channel (as in Fig. 5), to smaller values. On the bosonic side of the resonance ($B < B_0$), a Bose condensate of molecules appears at sufficiently large detuning from the resonance. The molecules interact with s-wave scattering length $0.6a$ [58]. The gas is extremely dilute: the interparticle distance is 3–4 orders of magnitude larger than the electrostatic potential scale r_0, which is a few tenths of a nanometer for lithium. The condition $a \gg r_0$ is easily satisfied. This justifies the exclusion of details of interparticle interactions from the problem, and the relation of all interaction processes to a single parameter, viz. the scattering length a.

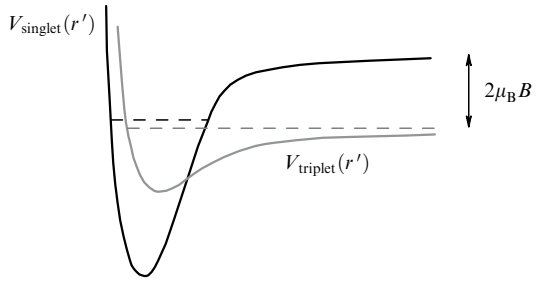

Figure 5. Fano–Feshbach resonance: unbound pair of particles in the triplet channel with energy marked by the gray dashed straight line comes into resonance with the energy of the singlet-channel bound state (black dashed straight line). Mutual location of the bound and unbound states in the figure corresponds to $a < 0$.

3.2 Parameterization of interactions for two-dimensional kinematics

The theory of two-dimensional systems traditionally has to do with the two-dimensional s-wave scattering length a_2 [59, 60]. The s-wave part of the wavefunction of two unbound atoms at large distances asymptotically behaves as $\psi_\perp(\rho') \propto \ln\rho'/a_2$ ($\rho' \equiv |\boldsymbol{\rho}'|$, $\boldsymbol{\rho}'$ is the vector passed between two atoms in the xy plane), while the energy of the bound state may be expressed via a_2 as $E_{\text{bound}} = -4\hbar^2/[ma_2^2\exp(2\gamma)]$, where $\gamma \simeq 0.577$ is Euler's constant. The quantity $a_2\sqrt{n_2}$ is a natural parameter of a many-body problem [41], where n_2 is the two-dimensional number density of particles in one of two equally populated spin states. In the parameter $a_2\sqrt{n_2}$, the spatial scale of interaction of two particles is divided by the mean interparticle separation. Values of $a_2\sqrt{n_2} \gg 1$ and $a_2\sqrt{n_2} \ll 1$ correspond to the fermionic and bosonic limits, respectively, while $a_2\sqrt{n_2} \sim 1$ is the region of strong interactions.

In experiments with ultracold atoms, the interaction potential size r_0 is much smaller than the quantization size $l_z \equiv \sqrt{\hbar/(2m\omega_z)}$. The interaction potential may be regarded as a three-dimensional δ-function on the scale of the problem. As a result, the interactions are quasi-two-dimensional rather than two-dimensional, because at distances $\ll l_z$ the wavefunction of colliding atoms is determined by three-dimensional scattering length a. Mathematically, the problem of such a collision is equivalent to that in a purely two-dimensional potential [61]. Here, a_2 may be uniquely expressed as a function of a, l_z, and the relative momentum of two atoms $\hbar q \equiv |\mathbf{p}_1 - \mathbf{p}_2|/2$, where $\mathbf{p}_1$ and $\mathbf{p}_2$ are the

momenta of the colliding atoms in the laboratory reference frame. For the sake of finding the dependence $a_2(a, l_z, q)$, one may notice that for both the two-dimensional and quasi-two-dimensional scatterings, the atomic-pair wavefunction at large distances takes the form

$$\psi_\perp(\boldsymbol{\rho}') \simeq \exp(\mathrm{i}\mathbf{q}\boldsymbol{\rho}') - f\,\frac{\exp(\mathrm{i}q\rho' - \mathrm{i}\pi/4)}{\sqrt{8\pi q\rho'}}\,. \tag{5}$$

Only the expressions for the amplitude f differ. For the purely two-dimensional problem, the amplitude is

$$f = f_{2\mathrm{D}}(q, a_2) \equiv -\frac{2\pi}{\ln\left[qa_2\exp\gamma/(2\mathrm{i})\right]}\,, \tag{6}$$

while for the quasi-two-dimensional one [61], the relevant expression is

$$f = f_{\mathrm{Q2D}}(q, a, l_z) \equiv \frac{2\pi}{\sqrt{\pi}\,l_z/a + w(q^2 l_z^2)/2}\,, \tag{7}$$

where function $w(\xi)$ is defined via the limit:

$$w(\xi) \equiv \lim_{J\to\infty}\left[\sqrt{\frac{4J}{\pi}}\ln\frac{J}{e^2} - \sum_{j=0}^{J}\frac{(2j-1)!!}{(2j)!!}\ln(j-\xi-\mathrm{i}0)\right]. \tag{8}$$

As a result, a_2 may be found from the relationship [41]

$$f_{\mathrm{Q2D}}(q, a, l_z) = f_{2\mathrm{D}}(q, a_2)\,. \tag{9}$$

In the limit $q \to 0$, this approach yields the known expression [61]

$$a_2 \simeq 2.96\,l_z\exp\left(-\frac{l_z\sqrt{\pi}}{a}\right), \tag{10}$$

where, we note, no break appears at the resonance, as a jumps from $-\infty$ to $+\infty$. In a many-body system, the momentum differs from zero, while the typical momentum scale may be expressed via the chemical potential μ: $\hbar q = \sqrt{2\mu m}$. Also, formula (10) shows that the interaction size in a two-dimensional gas may be controlled by changing either a or ω_z.

Thus, the two-dimensional and quasi-two-dimensional problems are related to each other. This lets us parameterize the atomic gas state, as well as the state of the molecular gas emerging from the atomic gas, via the quantity $a_2\sqrt{n_2}$. An opportunity appears to compare experimental data with purely two-dimensional models.

4. Reflection of statistics in the pressure at nearly zero temperature

4.1 Temperature measurement

The Fermi pressure is a direct consequence of the fermionic statistics, while the bosonic statistics causes the appearance of a collective wavefunction which may be detected by the interference. For revealing the Fermi pressure, the quantum effect has to be distinguished from a thermal one. For this purpose, we have to be sure that the temperature is close to zero.

The form of the trapped gas density profile serves as a source of information about the temperature. A two-dimensional number density profile similar to that of Fig. 4b is integrated along z, providing the one-dimensional density profile $n_1(x)$ averaged over 30 nearly identical clouds. An example of such a profile is demonstrated in Fig. 6a. For a high temperature, $T > E_{\mathrm{F}}$, the gas is close to a classical one, and its density profile is close to the Gaussian distribution. At $T = 0$, the edges of the distribution $n_1(x)$ are sharper, and the number density distribution has the form

$$n_1(x) = \begin{cases} \dfrac{8N}{3\pi R_x}\left(1 - \dfrac{x^2}{R_x^2}\right)^{3/2}, & \text{for } x < R_x\,, \\ 0\,, & \text{for } x > R_x\,, \end{cases} \tag{11}$$

where $R_x \equiv \sqrt{2\mu/(m\omega_x^2)}$ is the Thomas–Fermi radius. At an arbitrary temperature T, the number density profile of a nearly ideal Fermi gas is expressed as

$$n_1(x) = -\sqrt{\frac{m\omega_\perp}{2\pi\hbar}}\left(\frac{T}{\hbar\omega_\perp}\right)^{3/2}\mathrm{Li}_{3/2}\left[-\exp\left(\frac{\mu}{T} - \frac{m\omega_\perp^2 x^2}{2T}\right)\right], \tag{12}$$

where $\mathrm{Li}_{3/2}$ is the 3/2-order polylogarithmic function, and the chemical potential μ is to be found self-consistently from the

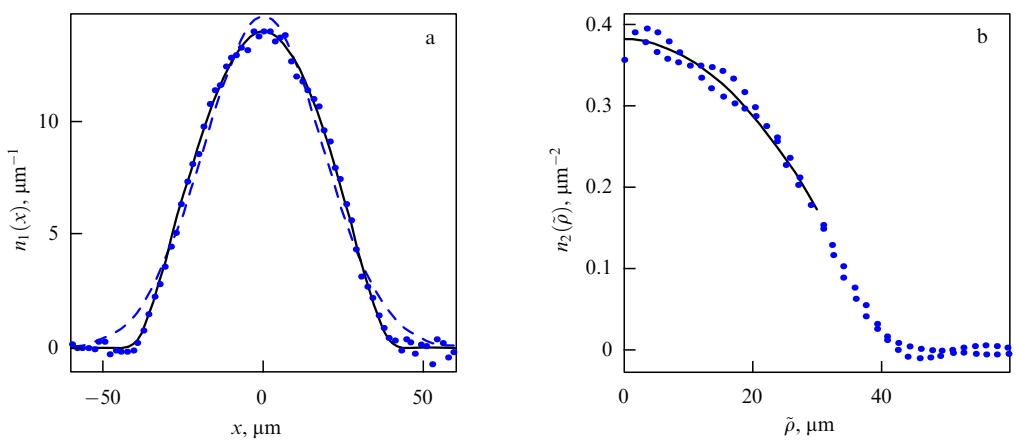

Figure 6. (Color online.) (a) Linear number density profile $n_1(x)$. Dots: data for $a_2\sqrt{n_2} = 55$, $B = 1400$ G, $\omega_x/(2\pi) = 94$ Hz, $\omega_y/(2\pi) = 141$ Hz, $\omega_z/(2\pi) = 6020$ Hz, and $N = 660$. Fits of the Thomas–Fermi (12) and Gaussian profile to the data are respectively shown by the solid and dashed curves. (b) Two-dimensional number density distribution in the xy plane, $n_2(\tilde{\rho})$, found from $n_1(x)$. Dots are the measured data. The curve is the fit of parabola $n_2(\tilde{\rho}) = n_2 - \tilde{\rho}^2 n_2''/2$ for finding the central number density $n_2 \equiv n_2(\tilde{\rho} = 0)$.

constraint $N = \int n_1(x)\,\mathrm{d}x$. By fitting this profile to the data of Fig. 6a, one may retrieve the temperature T. In experiments, temperatures $T \lesssim 0.1E_\mathrm{F}$ are accessible, which gives ≈ 10 nK in absolute units.

For comparison, an attempted fit by a Gaussian curve is shown in Fig. 6a. It can be seen that the Gaussian profile is off at both the edges and the center. For interacting Fermi and Bose gases, the number density profiles differ from profile (12). Despite this, since at $T = 0$ the dependence of the chemical potential on the number density is nearly quadratic ($\mu \propto n_2^2$) [62], the closeness of the density profile to distribution (11) firmly indicates deep degeneracy and smallness of the temperature with respect to E_F and chemical potential.

4.2 Pressure measurement

For studying the effects connected to quantum degeneracy, the system's properties at the center are especially interesting, because the gas is mostly degenerate there. The degree of degeneracy is determined by the ratio of the temperature to the local Fermi energy $\varepsilon_\mathrm{F}(x,y) \equiv 2\pi\hbar^2 n_2(x,y)/m$. The ratio $T/\varepsilon_\mathrm{F}(x,y)$ takes the smallest value at the cloud center. In addition, all known models are constructed for uniform systems. For quantitative comparison, therefore, we need measurements in the mostly uniform cloud part, which the cloud center is. While the imaging is done from a side and the cloud centers are not seen directly, it happens to be possible to measure the pressure and number density of particles at the cloud center.

The force balance equation is the basis for measuring the pressure at any cloud point:

$$\nabla_\perp P_2(x,y) = -n_2(x,y)\nabla_\perp V(x,y,0)\,, \tag{13}$$

where $P_2(x,y)$ is the partial pressure of each spin component. Integrating equation (13), we find that for a harmonic potential the central pressure is independent of the interaction: $P_2 = m\omega_\perp^2 N/(2\pi)$. To make the measurement more informative, we normalize the pressure to the local Fermi pressure, i.e., to the ideal Fermi gas pressure at $T = 0$ and at the same number density as in the cloud center: $n_2 \equiv n_2(0,0)$, $P_{2\,\mathrm{ideal}} = \pi n_2^2\hbar^2/m$. As a result, the value of $P_2/P_{2\,\mathrm{ideal}}$ close to unity would point to the fermionic character of the system, while a value much below unity would point to the bosonic nature.

Both quantities, n_2 and N, needed for finding $P_2/P_{2\,\mathrm{ideal}}$, are obtained from the $n_1(x)$ profile. The particle number N is found by integration. The number density profile $n_2(x,y)$ is fully reconstructed from the integral $n_1(x)$ owing to the cylindrical symmetry of potential (1) in stretched coordinates $(x, \tilde{y} \equiv y\,\omega_y/\omega_x)$. The inverse Abel transform yields

$$n_2(\tilde{\rho}) = -\frac{\omega_y/\omega_x}{\pi}\int_{\tilde{\rho}}^{\infty}\frac{\mathrm{d}n_1(x)}{\mathrm{d}x}\,\frac{\mathrm{d}x}{\sqrt{x^2-\tilde{\rho}^2}}\,, \tag{14}$$

where $\tilde{\rho} \equiv \sqrt{x^2+\tilde{y}^2}$. Profile $n_2(\tilde{\rho})$ is displayed in Fig. 6b. It is known that the inverse Abel transform emphasizes noise, especially on a small scale. To avoid noise in the $n_2(\tilde{\rho})$ distribution, we filter out small-scale noise in profile $n_1(x)$ prior to its substitution into formula (14). A fit of parabola $n_2(\tilde{\rho}) = n_2 - \tilde{\rho}^2 n_2''/2$ to the data near the origin yields the sought after quantity n_2.

4.3 Fermi-to-Bose crossover observation using the pressure

The pressure at the cloud center has been measured for the interaction parameter varying in a large interval. The results of measuring the normalized pressure at the cloud center, $P_2/P_{2\,\mathrm{ideal}}$, vs the interaction parameter are plotted in Fig. 7. The measurement destroys the quantum states of the system. Therefore, the system must be prepared for each measurement from the beginning.

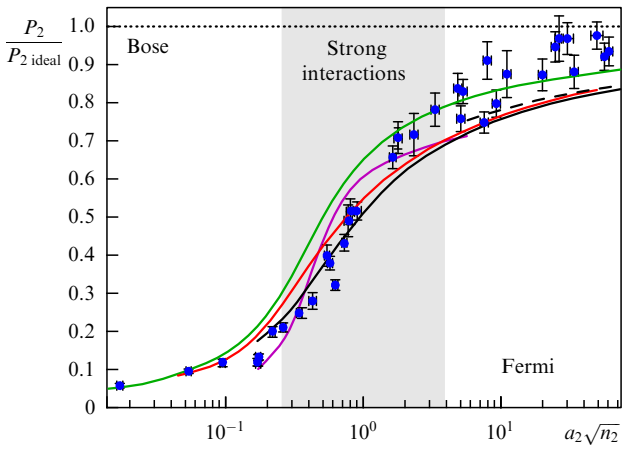

Figure 7. (Color online.) Normalized pressure at the cloud center vs the interaction parameter. Dots are the experimental data. Horizontal dotted line represents the mean-field Cooper-pair model [63]. Green curve is the mean-field model supplemented by fluctuations [30]. Dashed curve is the Fermi-liquid theory [60]. Purple solid curve traces a lattice Monte Carlo simulation [31]. Red curve is a diffusion Monte Carlo [28]. Black curve follows an auxiliary-field Monte Carlo [32].

The qualitative form of the normalized pressure dependence on the coupling parameter tells us that the system crosses over from fermionic statistics (on the right-hand side of Fig. 7) to bosonic statistics (on the left-hand side of Fig. 7). For $a_2\sqrt{n_2} \gg 1$, the pressure in the system closely approaches the Fermi pressure. Such high pressure cannot be explained by thermal effects, because the temperature is low. As the binding of the particles becomes stronger, the pressure decreases to values much below the Fermi pressure. The pressure measured in the Bose regime is due to weak repulsion between diatomic molecular bosons. The center of the strong-interaction region ($a_2\sqrt{n_2} = 1$) approximately corresponds to a pressure drop by a factor of 2.

In the Fermi region of $a_2\sqrt{n_2} \geqslant 5$, the temperature falls in the interval $T = (0.02{-}0.15)E_\mathrm{F}$. Meanwhile, at $a_2\sqrt{n_2} = 5$, the temperature of pair breaking is expected at $0.01E_\mathrm{F}$ [64], and even lower at higher $a_2\sqrt{n_2}$. Therefore, the superfluid phase is most probably absent in the Fermi regime and the system resides in the Fermi-liquid state.

5. Condensation in a gas of Bose molecules

Condensation is not possible in a two-dimensional ideal uniform Bose gas, because too many states are available near the zero energy. Meanwhile, the density of states behaves in a parabolic potential like the square root of energy, which makes condensation possible at temperature $T_\mathrm{c} = E_\mathrm{F}\sqrt{3}/\pi$. The interactions change the density of states and the condensation conditions, because at nearly zero temperature each molecule resides in the effective potential

$$V_\mathrm{eff}(x,y) = \frac{2m(\omega_x^2x^2+\omega_y^2y^2)}{2} + g_2\,\frac{\hbar^2}{2m}\,n_2(x,y)\,, \tag{15}$$

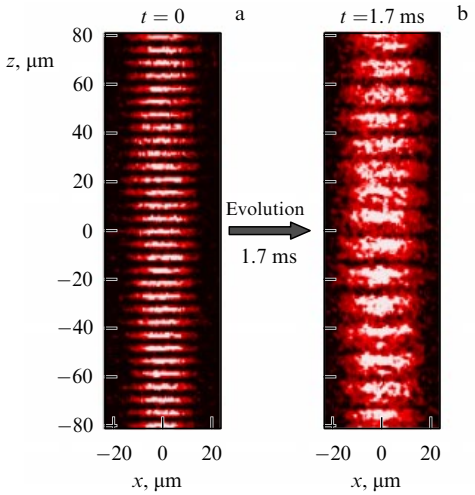

Figure 8. Interference of Li_2 molecule Bose condensates: (a) the initial state, where the condensates are in the traps, and (b) image in 1.7 ms after turn-off of the traps and free-space evolution.

which consists of the trap potential and the mean field of the ambient particles. The mean-field value is determined by the bosonic coupling parameter g_2. Potential $V_{\text{eff}}(x, y)$ is uniform in the whole area occupied by the cloud. Despite the uniformity of the potential, condensation is possible because of the finite size, which cuts off the long-wave fluctuations that would destroy condensation in an infinitely large system. With increasing repulsion g_2 between the bosons, the size of the cloud should increase, while the condensation temperature should decrease. This phenomenon has not been studied experimentally. The actual instance of condensation, however, has been established [41].

To detect the condensation in the Bose limit, the interference of the clouds has been observed upon their abrupt release from traps. A photo of the system at $t = 0$, prior to the release, is shown in Fig. 8a. Upon abrupt turn-off of the trapping potential at $t = 0$, the molecular gas evolves in the free space and may be observed at later instants t. The system after the evolution at $t = 1.7$ ms is shown in Fig. 8b. One may see straight interference fringes. This indicates that in each cloud there is a wavefunction whose phase is invariable across the cloud. Therefore, a Bose–Einstein condensate forms in each cloud.

In this case, the natural question is whether the condensates of separate clouds are independent from each other. Studies of the interference let us answer this question. If all clouds formed a common condensate, their phases would be equal. Therefore, a kind of Talbot effect [65] would be observed in the evolution: the system would reproduce its initial wavefunction along the z-axis at times that are integer multiples of the Talbot period

$$T_{\text{Talbot}} = \frac{m\lambda^2}{2\pi\hbar} = 1.7\ \text{ms}\,, \tag{16}$$

which would naturally appear in the course of evolution due to the initial period along the z-axis that equals $\lambda/2 = 5.3$ μm. In the analysis, one may neglect cloud expansion in the xy plane, because this is a slow process. Furthermore, when analyzing the evolution one may neglect the repulsion between the molecules, because the number density is small for most of the time. In addition to the evolution periodicity, the spacial period along the z-axis should be preserved.

In Fig. 8b representing the image at $t = T_{\text{Talbot}}$, a picture that qualitatively differs from the one expected within the Talbot effect can be seen. Instead of revival of the initial distribution along the z-axis, similar to the initial distribution in Fig. 8a, a spatial period that is two times bigger is seen. The qualitative difference with the Talbot effect indicates that phases of condensates are different and, consequently, condensates in adjacent clouds are independent.

6. Fermi-to-Bose crossover models

6.1 Mean-field Cooper-pair model for a three-dimensional system

For a three-dimensional system, a Fermi-to-Bose crossover theory may be constructed on the basis of the Bogoliubov superconductivity model with the Hamiltonian

$$\hat{H} = \sum_{\mathbf{k}} \frac{\hbar^2\mathbf{k}^2}{2m}\left(\hat{c}^{\dagger}_{\mathbf{k}\uparrow}\hat{c}_{\mathbf{k}\uparrow} + \hat{c}^{\dagger}_{\mathbf{k}\downarrow}\hat{c}_{\mathbf{k}\downarrow}\right) + g_3 \sum_{\mathbf{k},\mathbf{k}'} \hat{c}^{\dagger}_{\mathbf{k}\uparrow}\hat{c}^{\dagger}_{-\mathbf{k}\downarrow}\hat{c}_{-\mathbf{k}'\downarrow}\hat{c}_{\mathbf{k}'\uparrow}\,, \tag{17}$$

where the coupling constant g_3 is expressed via the three-dimensional scattering length: $g_3 = 4\pi\hbar^2 a/m$. The solution for the ground state in the form of the direct product of Cooper pairs, namely

$$\prod_{\mathbf{k}} \left(u_{\mathbf{k}} + v_{\mathbf{k}}\hat{c}^{\dagger}_{\mathbf{k}\uparrow}\hat{c}^{\dagger}_{-\mathbf{k}\downarrow}\right)|\text{vacuum}\rangle\,, \tag{18}$$

turned out to be applicable not just for small negative a, as in the initial problem statement, but for any value of a [49]. An analytical solution has been found [66], which shows that the change of $1/a$ from $-\infty$ to $+\infty$ brings about a decrease in the Cooper pair size, which eventually becomes much smaller than the interparticle distance. Such a course of things is not accompanied by any jumps in thermodynamic quantities. This solution qualitatively correctly reproduces the behavior of the pressure smoothly decreasing to zero.

6.2 Two-dimensional system's models

For a two-dimensional system, the use of a mean-field Cooper-pair model similar to Eqns (17) and (18) gives a qualitatively incorrect answer. While a two-body quantity, the two-fermion binding energy, shows qualitatively correct behavior implying its growth with strengthening the interaction [63], many-body quantities such as pressure, on the contrary, happen to be independent of the interaction. In particular, such a model predicts that the Fermi pressure must be present in the Bose limit. In Fig. 7, where the prediction of the mean-field Cooper-pair model [63] is shown by the dotted line, qualitative disagreement with the experimental data is seen.

The addition of fluctuations into the mean-field model yields the qualitatively correct dependence of the pressure on the interaction strength [30], shown by the green curve in Fig. 7. Indeed, according to the Ginzburg–Levanyuk criterion [26, 27], the reduction in the dimensionality is accompanied by an increasing role of fluctuations.

Models with a qualitatively correct description of the Fermi-to-Bose crossover have appeared only in a few recent years, such as model [30]. These models include quantum

diffusion Monte Carlo [28, 33], self-consistent T-matrix [29], finite-temperature lattice Monte Carlo [31], and auxiliary-field Monte Carlo simulations [32]. Predictions of some of these models are depicted in Fig. 7. Results of all models are given at $T = 0$. A quantitative discrepancy may be noted between the models.

Analytical models for the gas in the Bose [67] and Fermi [59, 60] asymptotes appeared much earlier. For a two-dimensional gas with s-wave interaction, it was possible to calculate the Fermi liquid theory from first principles [59, 60]. Starting from the results of Ref. [60], one may calculate the pressure:

$$\frac{P_2}{P_{2\,\mathrm{ideal}}} = 1 - \frac{1}{\ln\left(\sqrt{4\pi}a_2\sqrt{n_2}\right)} + \frac{0.787}{\left[\ln\left(\sqrt{4\pi}a_2\sqrt{n_2}\right)\right]^2}\,, \qquad (19)$$

which is plotted in Fig. 7 with the dashed curve. This analytical result agrees with the fixed-node diffusion Monte Carlo numerical calculation [28], but differs from the measurements. The discrepancy with the measurement is significant because, within the Fermi-liquid theory, the pressure is counted from the Fermi pressure rather than from zero. The difference between the experimental data and the Fermi-liquid theory [60] may be due to the mesoscopic character of the experimental system [41], because the calculation was done for an infinitely extended Fermi liquid. On the other hand, calculations within the mean-field model supplemented by fluctuations [30] agree better with the experimental data. The Fermi-liquid theory, which belongs to mean-field models, does not account for fluctuations; therefore, the additional pressure may be related to fluctuations in the two-dimensional system.

7. Conclusion

In experiments with the kinematically two-dimensional ultracold gas of Fermi atoms, states lying between the Bose and Fermi limits are observed. In all states, the gas is deeply degenerate. The condensate of diatomic molecular bosons serves as the Bose limit. The state may be judged from the pressure and the interference. The pressure drop in response to the tuning of the interaction indicates Fermi pressure disappearance and crossover into the Bose regime. The interference lets us see the appearance of the long-range order which unambiguously points to condensation. The pressure data may serve for quantitative testing of two-dimensional Bose and Fermi system models.

Acknowledgments

The authors acknowledge financial support from the Presidium of the Russian Academy of Sciences programs "Actual problems of low-temperature physics" and "Fundamental problems of nonlinear dynamics in mathematical and physical sciences", and from the Russian Foundation for Basic Research (grants 14-22-02080-ofi-m, 14-02-31681-mol_a, 15-02-08464, and 15-42-02638).

References

1. Fermi E *Rend. Lincei* **3** 145 (1926)
2. Dirac P A M *Proc. R. Soc. Lond. A* **112** 661 (1926)
3. Einstein A *Sitzungsber. Preuß. Akad. Wiss. Phys.-Math. Kl.* 3 (1925); Translated into Russian: *Sobranie Nauchnykh Trudov* Vol. 3 (Moscow: Nauka, 1966) p. 489
4. Sommerfeld A *Naturwissenschaften* **15** 824 (1927)
5. Kapitza P *Nature* **141** 74 (1938)
6. London F *Nature* **141** 643 (1938)
7. London F *Phys. Rev.* **54** 947 (1938)
8. Landau L D *J. Phys. USSR* **5** 71 (1941); *Zh. Eksp. Teor. Fiz.* **11** 592 (1941)
9. Bogolubov N *J. Phys. USSR* **11** 23 (1947); *Izv. Akad. Nauk SSSR Ser. Fiz.* **11** 77 (1947)
10. Nozières P, in *Bose–Einstein Condensation* (Eds A Griffin, D W Snoke, S Stringari) (Cambridge: Cambridge Univ. Press, 1995) p. 15
11. Keldysh L V, Kozlov A N *Sov. Phys. JETP* **27** 521 (1968); *Zh. Eksp. Teor. Fiz.* **54** 978 (1968)
12. Bogoliubov N N *Sov. Phys. JETP* **7** 41 (1958); *Zh. Eksp. Teor. Fiz.* **34** 58 (1958)
13. Bogoliubov N N *Sov. Phys. JETP* **7** 51 (1958); *Zh. Eksp. Teor. Fiz.* **34** 73 (1958)
14. Nozières P, Schmitt-Rink S *J. Low Temp. Phys.* **59** 195 (1985)
15. Kerbikov B *Surv. High Energy Phys.* **20** 47 (2006); hep-ph/0510302
16. Bartenstein M et al. *Phys. Rev. Lett.* **92** 120401 (2004)
17. Berezinskii V L *Sov. Phys. JETP* **34** 610 (1972); *Zh. Eksp. Teor. Fiz.* **61** 1144 (1971)
18. Kosterlitz J M, Thouless D J *J. Phys. C Solid State Phys.* **6** 1181 (1973)
19. Volovik G E, Yakovenko V M *J. Phys. Condens. Matter* **1** 5263 (1989)
20. Gurarie V, Radzihovsky L, Andreev A V *Phys. Rev. Lett.* **94** 230403 (2005)
21. Gu Z-C, Wang Z, Wen X-G *Phys. Rev. B* **91** 125149 (2015); arXiv:1010.1517
22. Prokof'ev N, Ruebenacker O, Svistunov B *Phys. Rev. Lett.* **87** 270402 (2001)
23. Dolgopolov V T *Phys. Usp.* **57** 105 (2014); *Usp. Fiz. Nauk* **184** 113 (2014)
24. Stormer H L, Tsui D C, Gossard A C *Rev. Mod. Phys.* **71** S298 (1999)
25. Kopaev Y V, Belyavskii V I, Kapaev V V *Phys. Usp.* **51** 191 (2008); *Usp. Fiz. Nauk* **178** 202 (2008)
26. Levanyuk A P *Sov. Phys. JETP* **9** 571 (1959); *Zh. Eksp. Teor. Fiz.* **36** 810 (1959)
27. Ginzburg V L *Sov. Phys. Solid State* **2** 1824 (1960); *Fiz. Tverd. Tela* **2** 2031 (1960)
28. Bertaina G, Giorgini S *Phys. Rev. Lett.* **106** 110403 (2011)
29. Bauer M, Parish M M, Enss T *Phys. Rev. Lett.* **112** 135302 (2014)
30. He L et al. *Phys. Rev. A* **92** 023620 (2015)
31. Anderson E R, Drut J E *Phys. Rev. Lett.* **115** 115301 (2015)
32. Shi H, Chiesa S, Zhang S *Phys. Rev. A* **92** 033603 (2015)
33. Galea A et al. *Phys. Rev. A* **93** 023602 (2016); arXiv:1511.05123
34. Sakai S et al. *Phys. Rev. Lett.* **111** 107001 (2013)
35. Pons J A, Viganò D, Rea N *Nature Phys.* **9** 431 (2013)
36. Loktev V M, Quick R M, Sharapov S G *Phys. Rep.* **349** 1 (2001)
37. Ruggeri M, Moroni S, Boninsegni M *Phys. Rev. Lett.* **111** 045303 (2013)
38. Martiyanov K, Makhalov V, Turlapov A *Phys. Rev. Lett.* **105** 030404 (2010)
39. Feld M et al. *Nature* **480** 75 (2011)
40. Sommer A T et al. *Phys. Rev. Lett.* **108** 045302 (2012)
41. Makhalov V, Martiyanov K, Turlapov A *Phys. Rev. Lett.* **112** 045301 (2014)
42. Boettcher I et al. *Phys. Rev. Lett.* **116** 045303 (2016); arXiv:1509.03610
43. Fenech K et al. *Phys. Rev. Lett.* **116** 045302 (2016); arXiv:1508.04502
44. Anderson M H et al. *Science* **269** 198 (1995)
45. O'Hara K M et al. *Science* **298** 2179 (2002)
46. Paredes B et al. *Nature* **429** 277 (2004)
47. Kraemer T et al. *Nature* **440** 315 (2006)
48. Bloch I, Dalibard J, Zwerger W *Rev. Mod. Phys.* **80** 885 (2008)
49. Giorgini S, Pitaevskii L P, Stringari S *Rev. Mod. Phys.* **80** 1215 (2008)
50. Balykin V I, Minogin V G, Letokhov V S *Rep. Prog. Phys.* **63** 1429 (2000)
51. Grimm R, Weidemüller M, Ovchinnikov Yu B *Adv. Atom. Mol. Opt. Phys.* **42** 95 (2000)

52. Luo L et al. *New J. Phys.* **8** 213 (2006)
53. Pitaevskii L P *Phys. Usp.* **51** 603 (2008); *Usp. Fiz. Nauk* **178** 633 (2008)
54. Chien C-C, Levin K *Phys. Rev. A* **82** 013603 (2010)
55. Houbiers M et al. *Phys. Rev. A* **57** R1497 (1998)
56. Chin C et al. *Rev. Mod. Phys.* **82** 1225 (2010)
57. Zürn G et al. *Phys. Rev. Lett.* **110** 135301 (2013)
58. Petrov D S, Salomon C, Shlyapnikov G V *Phys. Rev. Lett.* **93** 090404 (2004)
59. Bloom P *Phys. Rev. B* **12** 125 (1975)
60. Engelbrecht J R, Randeria M, Zhang L *Phys. Rev. B* **45** 10135 (1992)
61. Petrov D S, Shlyapnikov G V *Phys. Rev. A* **64** 012706 (2001)
62. Vogt E et al. *Phys. Rev. Lett.* **108** 070404 (2012)
63. Randeria M, Duan J-M, Shieh L-Y *Phys. Rev. Lett.* **62** 981 (1989)
64. Petrov D S, Baranov M A, Shlyapnikov G V *Phys. Rev. A* **67** 031601 (2003)
65. Talbot H F *Philos. Mag.* **6** 401 (1836)
66. Marini M, Pistolesi F, Strinati G *Eur. Phys. J. B* **1** 151 (1998)
67. Schick M *Phys. Rev. A* **3** 1067 (1971)